Instability of convection in a fluid layer rotating about an oblique axis

S. L. Pollicott, P. C. Matthews, and S. M. Cox
School of Mathematical Sciences, University of Nottingham, University Park, Nottingham NG7 2RD, United Kingdom
(Received 19 August 2002; published 9 January 2003)

We analyze thermal convection in a fluid layer confined between isothermal horizontal boundaries at which the tangential component of the fluid stress vanishes. The layer rotates about an oblique, nearly vertical axis. Using a model set of equations for w, the horizontal planform of the vertical velocity component, and ψ, a stream function related to a large-scale vertical vorticity field, we describe the instabilities of convection rolls. We show how the usual Küppers-Lortz instability, which leads to a continual precession of the roll pattern, can be suppressed by the oblique rotation vector. Of particular interest is the small-angle instability of rolls, to perturbations in the form of rolls that are almost aligned with the primary rolls; at finite Prandtl number, this instability is not prevented by the horizontal component of the rotation vector, unless this component is sufficiently strong, in which case stability is confined to small-amplitude rolls near the marginal stability boundary. A one-dimensional instability leading to amplitude-modulated rolls is unaffected by the oblique rotation. Numerical simulations of the model equations are presented, which illustrate the instabilities analyzed.

DOI: 10.1103/PhysRevE.67.016301 PACS number(s): 47.54.+r, 47.20.Bp, 47.27.Te, 47.20.Lz

I. INTRODUCTION

Convection in a horizontal fluid layer rotating about an oblique axis is the archetypal model problem for convection in planetary atmospheres. It also represents an interesting pattern formation problem, since the vertical and horizontal components of the rotation vector $\mathbf{\Omega}$ tend to have competing effects on the stability of convection rolls. First we recall that the *vertical* component Ω_v tends to lead to the Küppers-Lortz instability [1,2], which causes convection rolls to precess continually about the vertical in the same sense as $\mathbf{\Omega}$. However, the *horizontal* component $\mathbf{\Omega}_h$ tends to lead to a preference for rolls whose axes are aligned with $\mathbf{\Omega}_h$ (see, for example, Refs. [3–7]). In this paper we describe the influence of the competition between these two effects upon the stability of convection rolls, through asymptotic analysis and numerical simulation.

Of particular interest is the influence of a large-scale vertical vorticity mode upon the convection, which is investigated here in the analytically tractable case of ''ideal'' boundary conditions (in particular, zero tangential fluid stress at the boundaries), so that the large-scale mode is only weakly linearly damped. However, this mode is also known to play a significant role when more realistic, rigid, boundary conditions are adopted, even though its amplitude is significantly less in that case.

We analyze the convection through a pair of coupled nonlinear partial differential equations for the vertical velocity component w, and a stream function ψ that describes the large-scale motions. In these model equations, the dependence of the flow field upon the vertical coordinate z is factored out, so that the model directly involves the dependence of w and ψ upon only the horizontal coordinates x and y, and time. The model is based on that of Ponty, Passot, and Sulem [8], and is similar to other models, for example, Refs. [9–11].

We begin our analysis by studying the Küppers-Lortz instability of convection rolls, treating first the comparatively straightforward case of infinite Prandtl number, so that the large-scale vertical vorticity mode plays no significant role. Our broad conclusion is that rolls sufficiently well aligned with $\mathbf{\Omega}_h$ are stabilized to the Küppers-Lortz instability, provided $|\mathbf{\Omega}_h|$ is sufficiently great. Our results correct those of Roxin and Riecke [12].

When, by contrast, the Prandtl number is finite, the Küppers-Lortz instability is more complicated. The usual weakly nonlinear analysis of this instability proceeds by considering a ''primary'' set of rolls, with wave vector $\boldsymbol{k}_0$, perturbed by a ''secondary'' set of rolls, with wave vector $\boldsymbol{k}_1$. In the weakly nonlinear formulation near the onset of motion, where the Rayleigh number R is close to its critical value R_c, both $|\boldsymbol{k}_0|$ and $|\boldsymbol{k}_1|$ are roughly equal to the critical wave number k_c of the linear stability theory. Provided that the angle ϕ between $\boldsymbol{k}_0$ and $\boldsymbol{k}_1$ is not near 60° or 120°, the wave vectors $\boldsymbol{k}_0 \pm \boldsymbol{k}_1$ of the second-order harmonics lie away from the circle of critical wave vectors, i.e., they are not resonant, and their amplitudes are slaved to those of the primary and secondary rolls. However, when the angle ϕ is small, $|\boldsymbol{k}_0 - \boldsymbol{k}_1| \ll k_c$ and the corresponding harmonic generates a large-scale motion [2]. In the case of stress-free horizontal boundaries, as contemplated here, this motion is only weakly damped, and so must explicitly be included, together with the near-marginal mode with wave vector $2\boldsymbol{k}_0 - \boldsymbol{k}_1$, in the analysis of the instability in the small-ϕ limit. The treatment of this limit has been given elsewhere when the rotation vector is exactly vertical [13]: there it is found that when $(R - R_c)/R_c = O(\epsilon^2)$, where $0 < \epsilon \ll 1$, all rolls are unstable to perturbations oriented at an angle $\phi = O(\epsilon^{2/5})$, regardless of the vertical rotation rate. On the other hand, instability to either the usual Küppers-Lortz disturbances, which have $\phi = O(1)$, or to disturbances with $\phi \ll \epsilon^{2/5}$, requires that the vertical rotation rate exceed some threshold value. The effects of a weakly tilted rotation vector are explored below, and it is shown that some rolls (those of the smallest amplitude, farthest from being aligned with $\mathbf{\Omega}_h$) may be stabilized against the small-angle Küppers-Lortz instability.

To facilitate the analysis of the small-angle Küppers-Lortz

instability, we assume for algebraic convenience that $|\boldsymbol{k}_0| = |\boldsymbol{k}_1| = k_c$, although exact equality is not essential to the instability. If this assumption is relaxed, so that $|\boldsymbol{k}_0|, |\boldsymbol{k}_1| \approx k_c$, then a further instability is found, this time present even for the exact alignment between the original and the perturbing rolls (i.e., for $\phi = 0$), through an analog of the Eckhaus instability [14]. However, in the presence of nonzero Ω_v, this instability is essentially modified from the usual Eckhaus instability in two respects [15–17]. First, rather than being purely a phase instability, it may have a significant impact on the amplitude of the convection and can lead to a pattern of stable, strongly localized convection. Second, if Ω_v is sufficiently large, and the Prandtl number not too large, then *all* rolls may be susceptible to this instability at onset, generally leading to localization of the convection, to convection in a planform other than rolls, or to time-dependent convection.

There are, of course, many other instabilities to which the rolls may be susceptible, including the zigzag and skewed-varicose instabilities. A detailed analysis of these other instabilities is given by Pollicott [18].

Our analysis of the various instabilities is compared with numerical simulations in Sec. VI, which allow us to determine the nonlinear development of the instabilities.

II. MODEL EQUATIONS FOR ROTATING CONVECTION

In this section, we introduce a reduced two-dimensional model for rotating convection in a Boussinesq fluid. Such models have been widely used for studying convection [8–11] and have the advantage of greatly simplifying both analytical and numerical studies, while capturing the essential features of the convection.

Our model is essentially that of Ponty *et al.* [8], derived for the case $\boldsymbol{\Omega}_h = \mathbf{0}$, but with an additional linear term [6] reflecting the presence of a small horizontal component in the rotation vector. Its derivation is now briefly sketched. It is assumed that the parameters are such that the onset of convection is steady, and that the horizontal boundaries at the top and bottom of the fluid layer are stress-free and isothermal. The horizontal component of the rotation vector is chosen to point in the y direction, so $\boldsymbol{\Omega} = (0, \Omega_h, \Omega_v)$. The solution to the governing equations is then expanded in powers of a small parameter ϵ, proportional to the square root of the excess Rayleigh number, assuming that convection is close to onset and that $\Omega_h = O(\epsilon)$. As Ponty *et al.* [8] indicate, it is necessary to make some simplifying assumptions concerning the form of the solution at second order in order to complete the derivation of a relatively simple model. The price that we pay for this relative simplicity is that the resulting model equations are not strictly asymptotic, and involve terms of mixed asymptotic order. The final dimensionless equations involve the vertical velocity component $w(x,y,t)$, where the dependence on the depth of the fluid layer has been factored out, and a stream function $\psi(x,y,t)$ for the mean flow. It is a consequence of the slight deviation from a vertical rotation axis that the only influence of nonzero Ω_h is through an additional linear term in the equation for w; the form of this term was derived by Busse [6]. The model equations are

$$\tau w_t = [\epsilon^2 r - (1+\nabla^2)^2] w + \epsilon^2 \omega^2 w_{yy} - M w - \alpha_1 \boldsymbol{\nabla} w \cdot \boldsymbol{\nabla} M + \alpha_2 \hat{\boldsymbol{z}} \cdot \boldsymbol{\nabla} \times [|\boldsymbol{\nabla} w|^2 \boldsymbol{\nabla} w] - \alpha_3 \hat{\boldsymbol{z}} \cdot (\boldsymbol{\nabla} w \times \boldsymbol{\nabla} \psi) - \alpha_4 w \nabla^2 \psi - \alpha_5 \boldsymbol{\nabla} w \cdot \boldsymbol{\nabla} \nabla^2 \psi, \tag{1}$$

$$\nabla^2 \psi_t = \mathrm{Pr} \nabla^4 \psi + \alpha_0 \hat{\boldsymbol{z}} \cdot \boldsymbol{\nabla} \times (\boldsymbol{\nabla} w \nabla^2 w) + \alpha_6 \boldsymbol{\nabla} \cdot (\boldsymbol{\nabla} w \nabla^2 w), \tag{2}$$

where

$$M = w^2 + \boldsymbol{\nabla} w \cdot \boldsymbol{\nabla} w.$$

The parameter ω is proportional to Ω_h [6], and appears only in one linear term in Eq. (1); this term alone breaks the rotational invariance of the system. The parameters $\alpha_0, \ldots, \alpha_6$ and τ are functions of the Prandtl number Pr and the Taylor number, and r is a rescaled Rayleigh number [8]. The terms α_2, α_4, α_5, and α_6 are odd functions of Ω_v, and these terms break the reflection symmetry of the system. If $\Omega_v > 0$, then α_2 and α_5 are positive but α_4 and α_6 are negative. The model has the symmetry $w \to -w$, which is inherited from the up-down symmetry of the original problem.

This model shows similarities to other two-dimensional convection models that include a pattern mode w and a large-scale vorticity mode ψ. Unlike the models of Neufeld *et al.* [10] and of Cox [11], however, our model allows the large-scale mode to evolve in time, rather than be enslaved to the pattern mode w. Our model corresponds closely to that of Ponty *et al.* [8], but with the addition of the term in ω. As discussed by Roxin and Riecke [12], we can regard ω as representing any effect that breaks the isotropy of the system, such as an oblique rotation axis (as here), or a weak imposed flow.

The basic state of no motion is $w = \psi = 0$, and when linearized about this state Eqs. (1) and (2) decouple, so that a mode with wave vector $\boldsymbol{k} = (k,l)$ has growth rate λ_w or λ_ψ, where

$$\tau \lambda_w = \epsilon^2 r - (1 - |\boldsymbol{k}|^2)^2 - \epsilon^2 \omega^2 l^2, \tag{3}$$

$$\lambda_\psi = -\mathrm{Pr} |\boldsymbol{k}|^2. \tag{4}$$

In the isotropic case ($\omega = 0$) the modes of maximum growth rate are those on the circle $|\boldsymbol{k}|^2 = 1$, but for nonzero ω this situation is further restricted so that the mode of maximum growth rate occurs when $k = 1$, $l = 0$, i.e., for rolls with their axes aligned with the horizontal component of the rotation vector. For rolls that are not aligned, the mode of maximum growth rate has $|\boldsymbol{k}| = 1 + O(\epsilon^2)$.

On large horizontal scales, ψ is only weakly damped, reflecting the fact that a uniform flow is neutrally stable with stress-free boundaries. This near-neutral large-scale mean flow plays a crucial role in modulational instabilities of the convection [13,16,19].

In Sec. III we consider the simpler case of infinite Prandtl number, when ψ may be neglected. A more complicated general case is discussed in Sec. IV.

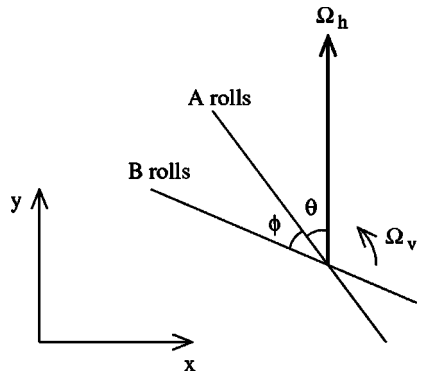

FIG. 1. Geometry of the axes of the *A* and *B* rolls in relation to the horizontal component of the rotation vector.

III. INFINITE PRANDTL NUMBER

In the limit of large Prandtl number Pr, ψ is strongly damped and models (1) and (2) reduce to the single equation

$$\tau w_t = [\epsilon^2 r - (1+\nabla^2)^2]w + \epsilon^2\omega^2 w_{yy} - w(w^2 + q\nabla w\cdot\nabla w) - \alpha_1\nabla w\cdot\nabla(w^2+\nabla w\cdot\nabla w) + \alpha_2\hat{\boldsymbol{z}}\cdot\nabla\times[(\nabla w\cdot\nabla w)\nabla w]. \quad (5)$$

Here we have introduced a parameter q, to facilitate comparison with the model of Roxin and Riecke [12] (for which we set $\tau=1$, $q=0$, $\alpha_1=0$); for our model, $q=1$.

For $\epsilon \ll 1$ we expand the solution to Eq. (5) as

$$w = \epsilon w_1 + \epsilon^2 w_2 + \epsilon^3 w_3 + \cdots,$$

and consider terms at successive orders of ϵ in Eq. (5). We consider the stability of one set of rolls (A) to a second set of rolls (B) whose axes lie at some angle ϕ to those of the A rolls. Thus

$$w_1 = \{A(T)e^{i(x\cos\theta + y\sin\theta)} + \text{c.c.}\} + \{B(T)e^{i[x\cos(\theta+\phi)+y\sin(\theta+\phi)]} + \text{c.c.}\}, \quad (6)$$

where $T=\epsilon^2 t$, representing rolls whose axes make angles θ and $\theta+\phi$ with the y axis, as shown in Fig. 1. We have assumed for simplicity that both sets of rolls have a wave vector on the critical circle $|\boldsymbol{k}|^2=1$. At $O(\epsilon^3)$ we find that A and B evolve according to

$$\tau A' = rA - \omega^2(\sin^2\theta)A - (3+q)A|A|^2 - 2[3+q+\alpha_2\sin 2\phi + \alpha_1(1-\cos 2\phi)]A|B|^2,$$

$$\tau B' = rB - \omega^2\sin^2(\theta+\phi)B - (3+q)B|B|^2 - 2[3+q - \alpha_2\sin 2\phi + \alpha_1(1-\cos 2\phi)]B|A|^2.$$

These equations collapse to those of Ref. [12] for the appropriate parameter values.

We now consider the stability of the A rolls to perturbations in the form of B rolls. With no loss of generality, the amplitude A may be taken to be real.

A. Küppers-Lortz instability for $\omega=0$ (isotropic case)

If $\omega=0$, the A rolls exist for $r>0$ and have amplitude A_0, where

$$A_0 = \sqrt{\frac{r}{3+q}}.$$

Perturbations to the amplitude of the A rolls are damped, but perturbations in the form of B rolls grow like $e^{\lambda T}=e^{\lambda\epsilon^2 t}$, where the growth rate λ satisfies

$$\frac{\tau\lambda}{r} = -1 + 2\frac{\alpha_2\sin 2\phi - \alpha_1(1-\cos 2\phi)}{3+q}. \quad (7)$$

For the Roxin and Riecke [12] case, Eq. (7) becomes

$$\frac{\lambda}{r} = -1 + \frac{2\alpha_2\sin 2\phi}{3}$$

and the maximum growth rate is thus achieved when $\phi=\pi/4$, giving rise to Küppers-Lortz instability if $\alpha_2>\alpha_{\text{KL}}\equiv\frac{3}{2}$.

In our more general case, from Eq. (7), λ is maximized when $\tan 2\phi=\alpha_2/\alpha_1$, and the condition for instability is

$$-1 + 2\frac{\sqrt{\alpha_1^2+\alpha_2^2}-\alpha_1}{3+q} > 0,$$

which can be written alternatively as

$$\alpha_2^2 > (3+q)^2/4 + \alpha_1(3+q).$$

These results are independent of the orientation of the original rolls, and show that rolls become unstable to the Küppers-Lortz instability if α_2 is sufficiently large.

B. Küppers-Lortz instability for $\omega\neq 0$

In the case $\omega\neq 0$, the A rolls exist for $r>\omega^2\sin^2\theta$ and have amplitude $A=A_0$, where

$$A_0 = \sqrt{\frac{r-\omega^2\sin^2\theta}{3+q}}.$$

Perturbations in A are still damped, but now perturbations in B have growth rate λ, where

$$\tau\lambda = -r - \omega^2\sin^2(\theta+\phi) + 2\omega^2\sin^2\theta + 2\frac{\alpha_2\sin 2\phi - \alpha_1(1-\cos 2\phi)}{3+q}(r-\omega^2\sin^2\theta). \quad (8)$$

It is instructive to begin our discussion of Eq. (8) by considering the region close to the marginal stability curve, where $0<A_0^2\ll 1$ (i.e., $0<r-\omega^2\sin^2\theta\ll 1$). Here the growth rate satisfies

$$\tau\lambda \sim \omega^2[\sin^2\theta - \sin^2(\theta+\phi)]. \quad (9)$$

Thus λ can be made *positive* by selecting

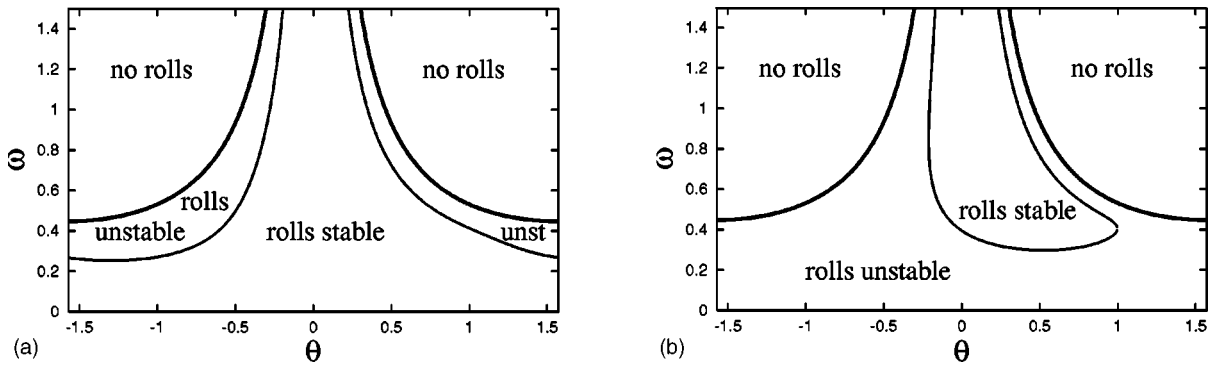

FIG. 2. Marginal stability curve (heavy line, delineating the region of existence of rolls) and stability regions, according to Eq. (14), with $r=0.2$ and (a) $\alpha_2=1$ or (b) $\alpha_2=2$. The stability of rolls to the Küppers-Lortz instability is indicated.

$$\phi \approx -\theta. \tag{10}$$

So, just inside the marginal stability curve, the rolls are *unstable*. This instability will be referred to as an *alignment* instability, since it tends to bring the most poorly aligned rolls closer into alignment with the horizontal component of the rotation vector.

Another special case of interest is the rolls with $\theta=0$, which are aligned with the horizontal component of the rotation vector. In this case, the growth rate of the Küppers-Lortz instability satisfies, from Eq. (8),

$$\tau\lambda = -r-\omega^2\sin^2\phi+2r\,\frac{\alpha_2\sin 2\phi-\alpha_1(1-\cos 2\phi)}{3+q}.$$

Comparing this expression with the corresponding expression (7) for $\omega=0$ shows that the growth rate is reduced when $\omega\neq 0$, in other words, the horizontal component of the rotation vector inhibits the Küppers-Lortz instability.

Returning to the general case, we seek, for rolls of a given orientation (i.e., a given value of θ), the most dangerous mode of instability, by maximizing λ over all ϕ in Eq. (8). We then consider the stability boundary, given by $\lambda_{\max}=0$. In the Roxin and Riecke [12] case

$$\lambda = r(-1+\tfrac{2}{3}\alpha_2\sin 2\phi)-\omega^2[\sin^2(\theta+\phi) + \tfrac{2}{3}(\alpha_2\sin 2\phi-3)\sin^2\theta]. \tag{11}$$

However, the stability boundaries plotted in Ref. [12], stemming from Eq. (11), are incorrect, since they are inconsistent with the result following from Eq. (9) showing that small-amplitude rolls are always unstable; we correct them below. In the general case (8), the growth rate λ is maximized when $\phi=\phi_{\max}$, where

$$\tan 2\phi_{\max}=\frac{4\alpha_2(r-\omega^2\sin^2\theta)-(3+q)\omega^2\sin 2\theta}{4\alpha_1(r-\omega^2\sin^2\theta)+(3+q)\omega^2\cos 2\theta}. \tag{12}$$

At this value of ϕ, the corresponding growth rate satisfies

$$\tau\lambda_{\max}=-r-\frac{\omega^2}{2}+2\omega^2\sin^2\theta-\frac{2\alpha_1}{3+q}(r-\omega^2\sin^2\theta) +\left[\left(\frac{2\alpha_2(r-\omega^2\sin^2\theta)}{3+q}-\frac{\omega^2\sin 2\theta}{2}\right)^2 +\left(\frac{2\alpha_1(r-\omega^2\sin^2\theta)}{3+q}+\frac{\omega^2\cos 2\theta}{2}\right)^2\right]^{1/2}, \tag{13}$$

where taking the positive square root ensures that this is the maximum value of λ (rather than the minimum). The stability boundary for rolls is then $\lambda_{\max}=0$.

For the parameter values appropriate to the model of Roxin and Riecke [12], Eq. (13) simplifies to

$$\lambda_{\max}=-r-\frac{\omega^2}{2}+2\omega^2\sin^2\theta+\left[\frac{\omega^4\cos^2 2\theta}{4} +\left(\frac{2\alpha_2(r-\omega^2\sin^2\theta)}{3}-\frac{\omega^2\sin 2\theta}{2}\right)^2\right]^{1/2}. \tag{14}$$

Figure 2 shows the stability region for rolls, derived from Eq. (14) when $r=0.2$, in two cases: $\alpha_2=1<\alpha_{\mathrm{KL}}$ and $\alpha_2=2>\alpha_{\mathrm{KL}}$. In the former case, Fig. 2(a), all rolls are stable to the Küppers-Lortz instability when $\omega=0$, and this forces the stability boundary to have the indicated topology. As ω is increased, rolls significantly out of alignment are the first to become unstable. By contrast, in the latter case, Fig. 2(b), all rolls are Küppers-Lortz-*unstable* when $\omega=0$, and hence the stability region has a different topology (it is closed at the bottom). Here ω must exceed some threshold before the tendency of rolls to align with ω can stabilize them against the Küppers-Lortz instability. Note that some rolls with positive θ are unstable for $\omega=0$, and as ω is increased, first become stable and then become unstable again. There are two physically distinct instability mechanisms acting here: the ''alignment'' instability, caused by the horizontal component of the rotation vector, and the Küppers-Lortz instability, caused by the vertical component. However, these two instabilities cannot be clearly distinguished since their growth rates are given by a single formula.

Regardless of the value of α_2 (provided it is nonzero), by virtue of the fact that the fluid layer has a vertical component

of rotation vector, we expect the stability boundary to be asymmetrical about $\theta=0$, since the α_2 term breaks the reflection symmetry of the system. This asymmetry is readily observed in the asymptotic form of the stability boundary for large ω, which is found from Eq. (14) to be

$$\theta=\frac{\pm\sqrt{r/2}}{\omega}+\frac{\alpha_2 r}{6\omega^2}+O(\omega^{-3}).$$

By contrast, the two sections of the marginal stability curve, between which rolls exist, are symmetrical and are given by

$$\theta=\frac{\pm\sqrt{r}}{\omega}+O(\omega^{-3}).$$

At leading order therefore, for large ω, the width of the region of stable rolls is narrower than the width of the region in which the rolls exist by a factor of $\sqrt{2}$. The same result holds for the more general stability boundary (13).

A further noteworthy consequence of the asymmetry of the stability boundary arises when it has the topology of Fig. 2(b). In this case, as ω is increased, the first rolls to be stabilized to the Küppers-Lortz instability are not those aligned with $\mathbf{\Omega}_h$; instead, the minimum of the stability boundary corresponds to the rolls with some positive value of θ. This preference illustrates a balance between the physical influences of the two components of $\mathbf{\Omega}$, one tending to force alignment with the y axis, the other tending to turn rolls counterclockwise. It is not possible to write down a simple analytical expression for this preferred value of θ in general, but when α_2 just exceeds the threshold value α_{KL}, it is readily determined that the stability boundary takes the form

$$\omega^2\sim\frac{2(\alpha_2/\alpha_{\mathrm{KL}}-1)r}{\cos 2\theta+\sin 2\theta},$$

and hence that the first rolls to be stabilized to the Küppers-Lortz instability have

$$\theta\sim\tfrac{1}{2}\tan^{-1}1=\tfrac{1}{8}\pi\approx 0.39.$$

Results for the more general stability boundary (13) show the same qualitative features as discussed above and as shown in Fig. 2. Further details are given in Ref. [18].

IV. FINITE PRANDTL NUMBER

We now turn to the more complicated case of finite Prandtl number Pr, so the governing equations are Eqs. (1) and (2), and proceed as in the case $\mathrm{Pr}=\infty$, but also expanding the mean flow, so that

$$w=\epsilon w_1+\epsilon^2 w_2+\cdots,\quad \psi=\epsilon^2\psi_2+\cdots. \tag{15}$$

As when $\mathrm{Pr}=\infty$, w_1 takes the form Eq. (6) and $w_2=0$. By considering the terms at $O(\epsilon^2)$ we find

$$\begin{aligned}\psi_2=&\{\psi^+(T)e^{i\{x[\cos\theta+\cos(\theta+\phi)]+y[\sin\theta+\sin(\theta+\phi)]\}}+\text{c.c.}\}\\&+\{\psi^-(T)e^{i\{x[\cos\theta-\cos(\theta+\phi)]+y[\sin\theta-\sin(\theta+\phi)]\}}+\text{c.c.}\}\\&+\{\psi^\theta(T)e^{2i(x\cos\theta+y\sin\theta)}+\text{c.c.}\}\\&+\{\psi^\phi(T)e^{2i(x\cos(\theta+\phi)+y\sin(\theta+\phi))}+\text{c.c.}\},\end{aligned}$$

where

$$\psi^+=-\frac{\alpha_6 AB}{2\mathrm{Pr}(1+\cos\phi)},$$

$$\psi^-=-\frac{\alpha_6 AB^*}{2\mathrm{Pr}(1-\cos\phi)},$$

$$\psi^\theta=-\frac{\alpha_6 A^2}{8\mathrm{Pr}},$$

$$\psi^\phi=-\frac{\alpha_6 B^2}{8\mathrm{Pr}}.$$

At $O(\epsilon^3)$ in Eq. (1) we find that A and B now evolve according to

$$\tau A'=rA-\omega^2(\sin^2\theta)A-aA|A|^2-b^+A|B|^2,$$

$$\tau B'=rB-\omega^2(\sin^2(\theta+\phi))B-aB|B|^2-b^-B|A|^2,$$

where

$$a=4+\left(\frac{\alpha_4+2\alpha_5}{2\mathrm{Pr}}\right)\alpha_6 \tag{16}$$

and

$$b^\pm=2[4\pm\alpha_2\sin 2\phi+\alpha_1(1-\cos 2\phi)]+2\left(\frac{\alpha_4+\alpha_5}{\mathrm{Pr}}\right)\alpha_6 \mp\frac{\alpha_3\alpha_6\sin 2\phi}{\mathrm{Pr}(1-\cos 2\phi)}.$$

Let us now consider the A-rolls having amplitude $A=A_0$, where

$$A_0=\sqrt{\frac{r-\omega^2\sin^2\theta}{a}}. \tag{17}$$

Their stability is determined by the growth rate λ of perturbations to the B-rolls, which satisfies

$$\tau\lambda=r-\omega^2\sin^2(\theta+\phi)-b^-A_0^2. \tag{18}$$

Analysis of this expression for λ is in general rather complicated. In the limit $\mathrm{Pr}\to\infty$, Eq. (18) reduces to (8); for finite Pr the region of stability of rolls is modified. Figure 3 shows the growth rate as a function of ϕ for a typical case. Note that the growth rate has a maximum at a finite value of ϕ, but diverges as $\phi\to 0$. This divergence is a generic feature of the Küppers-Lortz instability with stress-free boundaries [2,8,13]. Rolls are always unstable to small-angle perturbations, and the introduction of a horizontal component of the

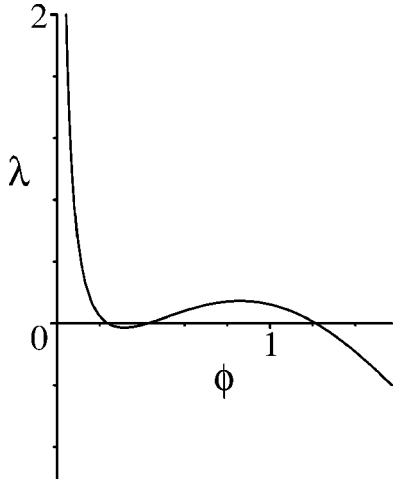

FIG. 3. Growth rate as a function of ϕ, according to Eq. (18), when $\tau=1.081$, $\alpha_0=0.718$, $\alpha_1=-0.4$, $\alpha_2=2.0$, $\alpha_3=8.650$, $\alpha_4=-0.557$, $\alpha_5=0.03712$, $\alpha_6=-0.696$ (corresponding to a Prandtl number of 10 and a Taylor number of 40), $r=1$, $\omega=0.59$, $\theta=0.9$.

rotation vector does not appear to prevent this instability (except for the rolls very close to the marginal curve—see Sec. IV A).

In what follows, we shall be particularly concerned with the limit $\phi\to 0$, in which the original rolls and the perturbing rolls are almost in alignment with each other. We therefore note at this point that the coefficients ψ^+, ψ^θ, and ψ^ϕ are all bounded in this limit, but that the large-scale mean-flow component ψ^- is singular, with

$$\psi^- \sim -\frac{\alpha_6 AB^*}{\mathrm{Pr}}(\phi^{-2}+\tfrac{1}{12}+\tfrac{1}{240}\phi^2+\cdots),$$

indicating that the calculation needs to be considered more carefully when ϕ is small. In the limit $\phi\to 0$, we find from this analysis that

$$\tau\lambda \sim -\frac{\alpha_3\alpha_6 A_0^2}{\mathrm{Pr}\phi}. \tag{19}$$

This breakdown in the theory reflects our incorrect treatment of the mode ψ^-, which is treated as slaved to the A and B modes; whereas when these two sets of rolls are almost aligned, this mode is dynamically significant in its own right.

A. The limit of nearly aligned rolls

In order to resolve the divergence of the growth rate for the instability of one set of the rolls to a second set, nearly aligned with the first, we need to consider three perturbations of significance, as illustrated in Fig. 4. We simplify the following analysis by assuming that both the original rolls and one of the perturbing rolls have critical wave numbers. We thus consider the stability of the A_0 rolls with wave vector (k,l), where

$$k^2+l^2=1, \tag{20}$$

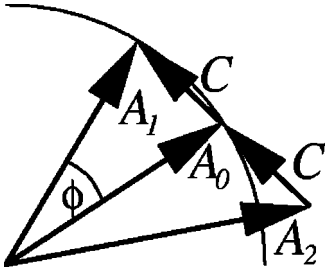

FIG. 4. Wave vectors of the significant modes for an analysis of the small-angle instability at finite Prandtl number. Part of the circle of critical wave vectors is shown. The important modes when ϕ is $O(1)$ are the original rolls A_0 and the perturbing rolls A_1 (both with critical wave numbers, for analytical convenience). In addition, when ϕ is small, other significant modes are C, the large-scale mode driven by interactions of A_0 and A_1 rolls, and A_2, perturbing rolls (with nearly critical wavenumber) driven by interactions of the A_0 rolls and C mode, or by cubic interactions of A_0 and A_1 rolls.

to perturbations with wave vectors $(k+m,l+n)$ (A_1 rolls), $(k-m,l-n)$ (A_2 rolls), (m,n) (C mode), where

$$(k+m)^2+(l+n)^2=1. \tag{21}$$

In our prior notation,

$$k=\cos\theta, \quad k+m=\cos(\theta+\phi),$$
$$l=\sin\theta, \quad l+n=\sin(\theta+\phi). \tag{22}$$

In view of Eqs. (20) and (21), it follows that

$$2(km+ln)+m^2+n^2=0. \tag{23}$$

Then from Eq. (22), it follows that $\sin\phi=kn-lm$. To study nearly aligned rolls, we suppose that ϕ is small and hence so are the wave numbers m and n; in this limit, $\phi\sim kn-lm\sim(m^2+n^2)^{1/2}$.

It is not possible to write down self-consistent nonlinear amplitude equations for modes A_0, A_1, A_2, and C as in the preceding section. This is because, for small ϕ, the interaction of the C mode with each of the A modes generates a further near-marginal A mode. Instead, we consider the A_0 mode to be the basic state and the other modes to be small perturbations; it is then possible to derive asymptotically self-consistent linearized equations for the perturbations.

In order to determine the stability of rolls, we consider expanding a solution to Eqs. (1) and (2) in the form

$$w=\{\epsilon A_0 e^{i(kx+ly)}+\delta A_1(T)e^{i[(k+m)x+(l+n)y]} + \delta A_2(T)e^{i[(k-m)x+(l-n)y]}\}+\text{c.c.}+\cdots,$$
$$\psi=\delta C(T)e^{i(mx+ny)}+\text{c.c.}+\cdots,$$

where δ is an infinitesimal quantity, and A_1, A_2, and C represent perturbations to the rolls, whose amplitude is given by

$$A_0=\sqrt{\frac{r-\omega^2 l^2}{a}}. \tag{24}$$

Although a variety of small-ϕ scalings is necessary in order to describe fully the stability of the A_0 rolls, the most important is the scaling that allows a matching to the apparently divergent Küppers-Lortz result (19), resolves the divergence of the growth rate, and contains the maximum growth rate. When $\omega=0$, as shown by Cox and Matthews [13], the appropriate scaling is

$$m,n=O(\epsilon^{2/5}), \tag{25}$$

$$km+ln=O(\epsilon^{4/5}), \tag{26}$$

$$A_1,A_2=O(1), \tag{27}$$

$$C=O(\epsilon^{1/5}), \tag{28}$$

with a growth rate

$$\lambda=O(\epsilon^{8/5}). \tag{29}$$

If we adopt this scaling for the present problem, in which ω does not necessarily vanish, we find that A_1, A_2, and C satisfy

$$\tau\lambda A_1=\alpha_3 A_0(kn-lm)C,$$

$$\tau\lambda A_2=-4(m^2+n^2)^2A_2-\alpha_3 A_0(kn-lm)C,$$

$$0=\mathrm{Pr}(m^2+n^2)^2C+\alpha_6(kn-lm)^2A_0(A_1+A_2),$$

independent of ω. Thus the growth rate λ satisfies

$$\tau^2\lambda^2+4\tau\lambda(m^2+n^2)^2+\frac{4\alpha_3\alpha_6}{\mathrm{Pr}}(kn-lm)^3A_0^2=0. \tag{30}$$

The scalings (25)–(29) allows us to match the apparently divergent growth rate of the Küppers-Lortz analysis in the limit $\phi\to 0$ to a regular, nondivergent expression valid at small angles between the original and perturbing rolls, since taking the limit $m^2+n^2\to\infty$ in Eq. (30) gives

$$\tau\lambda\sim-\frac{\alpha_3\alpha_6A_0^2(kn-lm)^3}{\mathrm{Pr}(m^2+n^2)^2}\sim-\frac{\alpha_3\alpha_6A_0^2}{\mathrm{Pr}\phi}, \tag{31}$$

which agrees with the divergent small-angle limit (19) of the Küppers-Lortz instability obtained above. Hence, as described in Ref. [13] for the case $\omega=0$, *all* rolls are unstable in this scaling. While one might have expected the presence of a nonzero horizontal component of the angular velocity vector to exert a stabilizing influence on rolls with appropriate orientation, its magnitude here is too small to do so [its contribution to the growth rate is $O(\epsilon^2)$, which is asymptotically smaller than the growth rate (29) found here].

Increasing the magnitude of ω stabilizes some of the rolls, as we now demonstrate. We begin by noting that the instability in Eq. (30) is forced by the term

$$\frac{4\alpha_3\alpha_6}{\mathrm{Pr}}(kn-lm)^3A_0^2.$$

Rolls might thus escape instability if this term could somehow be made smaller than the scalings (25)–(29) suggest. For example, near the edge of the region of existence of the original rolls, their amplitude A_0, and hence this instability-generating term, is small. Thus we now explore how to rescale quantities so as to include both the ''small-angle'' Küppers-Lortz instability illustrated in Eq. (31) and the alignment instability of nonzero ω [illustrated in Eq. (9) for $\mathrm{Pr}=\infty$]. It turns out that in order to introduce stabilizing terms, ω must be large and so l must be small, to maintain the asymptotic balance $\omega l=O(1)$ implicit in Eq. (24).

The actual derivation of the new scalings is rather algebraically involved. We proceed by considering the terms that arise in equations for the quantities $\tau d(A_1+A_2)/dt$, $\tau d(A_1-A_2)/dt$ and dC/dt. We choose a scaling so as to ensure the presence of certain terms that will give a balance between the small-angle instability described above, and in more detail by Cox and Matthews [13], and the tendency to align with nonzero ω. A considerable amount of trial and error is suppressed in the following description. In the equation for $\tau d(A_1+A_2)/dt$, the key terms are proportional to

$$\epsilon^2\omega^2n^2(A_1+A_2),\quad \epsilon^2\omega^2ln(A_1-A_2),\quad n^4(A_1-A_2). \tag{32}$$

Likewise, in the equation for $\tau d(A_1-A_2)/dt$, the key terms are proportional to

$$\epsilon^2\omega^2n^2(A_1-A_2),\quad \epsilon A_0nC. \tag{33}$$

Finally, in the equation for dC/dt, the time derivative itself is asymptotically smaller than those terms retained, of which the key terms are

$$\mathrm{Pr}n^4C,\quad \epsilon n^2A_0(A_1+A_2). \tag{34}$$

With no loss of generality, we specify the order of one of the perturbation quantities by setting $A_1-A_2=O(1)$. Then, by balancing the terms indicated, we find

$$l=O(\epsilon^{2-3\gamma}),$$

$$n=O(\epsilon^{\gamma}),$$

$$m=O(\epsilon^{2\gamma}),$$

$$\omega=O(\epsilon^{3\gamma-2}),$$

$$A_0=O(\epsilon^{(13\gamma-6)/2}),$$

$$A_1+A_2=O(\epsilon^{2(1-2\gamma)}),$$

$$A_1-A_2=O(1),$$

$$C=O(\epsilon^{\gamma/2}),$$

with $k-1\sim-\frac{1}{2}l^2$, where γ must lie in the range $6/13<\gamma<1/2$ so that terms omitted from Eqs. (32)–(34) remain asymptotically smaller than those retained. Correspondingly, the growth rate is

$$\lambda = O(\epsilon^{8\gamma-2}).$$

Note that the balance $\omega^2 l^2 = O(1)$ is retained, consistent with the scaling implied by expressions such as Eq. (24), where we have used Eq. (22).

The governing equations at $O(\epsilon^{4\gamma})$, $O(\epsilon^{8\gamma-2})$ and $O(\epsilon^{9\gamma/2})$, respectively, i.e., leading order in each case, are

$$\tau\lambda(A_1+A_2) = -\epsilon^2\omega^2 n^2(A_1+A_2) - (2\epsilon^2\omega^2 ln + 4n^2 m) \times (A_1 - A_2),$$

$$\tau\lambda(A_1-A_2) = -\epsilon^2\omega^2 n^2(A_1-A_2) + 2\epsilon\alpha_3 A_0 nC,$$

$$0 = \mathrm{Pr} n^4 C + \epsilon\alpha_6 n^2 A_0 (A_1+A_2).$$

Thus the growth rate λ satisfies

$$\tau^2\lambda^2 + 2\epsilon^2\omega^2 n^2\tau\lambda + \epsilon^4\omega^4 n^4 - \frac{4\epsilon^2(\epsilon^2\omega^2 l + 2mn)\alpha_3\alpha_6 A_0^2}{\mathrm{Pr}} = 0. \tag{35}$$

In analyzing the stability of these small-amplitude rolls according to Eq. (35), we first note that there can be no oscillatory instability because if the imaginary part λ_i is nonzero then the real part $\lambda_r = -\epsilon^2\omega^2 n^2/\tau \leqslant 0$. Thus in our examination of instability, we restrict attention to the case of real λ.

For a given set of rolls, we aim to maximize λ over n (with $2m + n^2 = 0$ to this order). For this purpose we introduce

$$\Lambda = \tau\lambda$$

and

$$Q = \frac{\mathrm{Pr}}{4\epsilon^2(-\alpha_3\alpha_6)A_0^2} > 0 \tag{36}$$

so that the scaled growth rate Λ satisfies

$$\Lambda^2 + 2\epsilon^2\omega^2 n^2\Lambda + \epsilon^4\omega^4 n^4 + \frac{\epsilon^2\omega^2 l - n^3}{Q} = 0.$$

From this formula it is immediately apparent that rolls with $l<0$ are unstable, but that rolls with $l>0$ are stable to perturbations with either small or large values of n. We now seek to determine whether any rolls with $l>0$ may be stable to *all* perturbations, regardless of n. It is readily determined that Λ takes its maximum value $\Lambda_{\max}$ when $n = n_{\max}$, which satisfies

$$n_{\max}^3 - \frac{9n_{\max}^2}{16\epsilon^4\omega^4 Q} = \epsilon^2\omega^2 l, \tag{37}$$

with

$$\Lambda_{\max} = -\epsilon^2\omega^2 n_{\max}^2 + \frac{3n_{\max}}{4\epsilon^2\omega^2 Q}. \tag{38}$$

The expressions (37) and (38) can profitably be analyzed by noting that the boundary $\Lambda_{\max}=0$ between the stable and unstable rolls arises when

$$n_{\max} = \frac{3}{4\epsilon^4\omega^4 Q}$$

and hence the threshold corresponds to rolls with wave number $l = l_c$, where

$$l_c = \frac{27}{256\epsilon^{14}\omega^{14}Q^3}.$$

In view of Eqs. (24) and (36), this equation gives l_c only implicitly, and it is somewhat more revealingly written as

$$r - \omega^2 l_c^2 = \left(\frac{4a^3\epsilon^8\omega^{14}P^3 l_c^3}{27(-\alpha_3\alpha_6)^3}\right)^{1/3}. \tag{39}$$

Since the term on the right-hand side of Eq. (39) is small, we may approximate l_c by $\sqrt{r}/\omega$ in this term, leading to

$$l_c \sim \frac{\sqrt{r}}{\omega} - \frac{(4\epsilon^8\omega^8)^{1/3} a\,\mathrm{Pr}}{6(-\alpha_3\alpha_6)}. \tag{40}$$

This indicates the location of the stable rolls just inside the marginal stability boundary and shows how the width of the band of stable rolls increases as ω increases. [The alternative case $n_{\max}=0$, which appears from Eq. (38) to offer the prospect of also giving $\Lambda_{\max}=0$, is ruled out since, by Eq. (37), it can apply only to $l=0$; however, when $l=0$, Λ is in fact maximized for $n_{\max}=9/16\epsilon^4\omega^4 Q$, giving $\Lambda_{\max} = 27/256\epsilon^6\omega^6 Q^2 > 0$, and instability.] By analyzing $\Lambda_{\max}$ near $l = l_c$, we find that

$$\Lambda_{\max} = -\frac{8\epsilon^8\omega^8 Q}{9}(l-l_c) + O((l-l_c)^2)$$

as $l - l_c \to 0$. Thus rolls are predicted to be stable for l just greater than l_c, i.e., for

$$l_c < l < \frac{\sqrt{r}}{\omega}.$$

Such a conclusion differs qualitatively from that found above for the case $P=\infty$, where rolls near the marginal curve are *unstable*. The resolution of this apparent discrepancy is not immediately obtained by taking the limit $\mathrm{Pr}\to\infty$ in Eq. (39), since we then find $l_c = 0$, which suggests that all rolls with $l>0$ are stable in this limit. However, this conclusion is unwarranted, since further scalings would need to be considered to address properly the limit $\mathrm{Pr}\to\infty$ [we can see this by noting, from (38), that our computed maximum growth rate $\Lambda_{\max}$ becomes small in this limit, and hence additional terms must be included].

In this analysis of the small-angle Küppers-Lortz instability we have assumed that both the A_0 rolls and the A_1 rolls have exactly critical wave number. This assumption, while

not crucial to the presence of the instability, yields considerable analytical simplifications. However, the assumption is too restrictive to capture a further instability that manifests itself when the A_0 and A_1 rolls are in extremely close alignment, in which case it must be relaxed. This instability is analyzed in the following section.

V. ONE-DIMENSIONAL MODULATIONAL INSTABILITY

In the limit of extremely close alignment between the original and the perturbing rolls, the above scalings need reconsideration, in order to permit analysis of an Eckhaus-like instability [14–17]. Here we allow the wave vector of the original rolls to lie slightly off the critical circle and (m,n) to be roughly parallel to (k,l) (rather than roughly perpendicular, as in the preceding section), so that

$$kn-lm \ll km+ln \ll 1, \tag{41}$$

rather than the scalings leading to Eq. (30). From eq. (41) combined with $k^2+l^2\sim 1$ it follows that

$$\frac{(km+ln)^2}{m^2+n^2}\sim 1.$$

In the absence of the large-scale mode ψ, such considerations yield the well-known Eckhaus instability; however, its characteristics are significantly modified by the presence of the slowly damped vertical vorticity mode [15,16]. In particular, whereas the Eckhaus instability involves distortions to the phase of the pattern, the corresponding instability here distorts both the phase and the amplitude.

Near the onset, we consider a basic state of rolls in which

$$w=\epsilon A_0 e^{i(kx+ly+\epsilon px+\epsilon qy)}+\cdots, \quad \psi=0$$

with $k^2+l^2=1$. The amplitude of these rolls is, to leading order in ϵ,

$$A_0=\sqrt{\frac{r-\omega^2 l^2-4(kp+lq)^2}{a}},$$

where a is given in Eq. (16).

The stability of the rolls is investigated by writing

$$w=\epsilon(A_0+V(T)e^{i\epsilon(mx+ny)} + W^*(T)e^{-i\epsilon(mx+ny)})e^{i(kx+ly+\epsilon px+\epsilon qy)}+\text{c.c.}+\cdots,$$

$$\psi=U(T)e^{i\epsilon(mx+ny)}+\text{c.c.}+\cdots,$$

where $T=\epsilon^2 t$, and by linearizing in the small disturbance amplitudes U, V and W.

At $O(\epsilon^3)$ in Eq. (1) and $O(\epsilon^4)$ in Eq. (2), respectively, we find that

$$\tau V' = -aA_0^2(V+W)+\alpha_4 A_0(m^2+n^2)U-4(km+ln) \times[2(kp+lq)+(km+ln)]V,$$

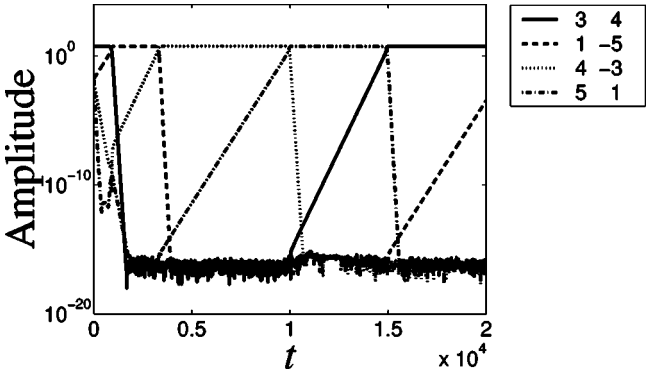

FIG. 5. Nonlinear evolution of mode amplitudes under the Küppers-Lortz instability in Eq. (5), with $\omega=0$ and $\alpha_2=2$. The instability continues indefinitely, forming a heteroclinic cycle.

$$\tau W' = -aA_0^2(V+W)+\alpha_4 A_0(m^2+n^2)U +4(km+ln)[2(kp+lq)-(km+ln)]W,$$

$$U' = -\Pr(m^2+n^2)U+\alpha_6 A_0(V+W).$$

Although, in principle, this system allows both oscillatory and monotonic instabilities, we find in practice that the monotonic instability is observed, and for small values of m and n. The condition for instability in the limit $m,n\to 0$ is readily found to be

$$A_0^2[\alpha_6(\alpha_4-2\alpha_5)-8\Pr]+16\Pr(kp+lq)^2>0. \tag{42}$$

In particular, *all* rolls are unstable if

$$\alpha_6(\alpha_4-2\alpha_5)>8\Pr.$$

Since $\alpha_6\alpha_4>0$ and $\alpha_6\alpha_5<0$, all rolls are unstable to the one-dimensional instability of Matthews and Cox [15] at sufficiently small Prandtl number. This instability is not prevented by the horizontal component of the rotation vector ω; the only effect of ω is to reduce the amplitude of the rolls, if they happen not to be aligned with the y axis.

It is straightforward to see that the stability boundary for this instability reduces to that for the usual Eckhaus instability when the effects of the coupling to the large-scale mode become negligible, e.g., when $\alpha_6\to 0$ or $\Pr\to\infty$. In this limit, the familiar factor-of-three difference between the expressions for the marginal and Eckhaus stability boundaries becomes clear if the condition (42) for instability is written in the form

$$r-\omega^2 l^2=12(kp+lq)^2,$$

which should be compared with the corresponding expression

$$r-\omega^2 l^2=4(kp+lq)^2$$

for the marginal stability boundary.

TABLE I. Comparison between numerical and theoretical stability thresholds for rolls in various alignments, for cases where $\alpha_2 < \alpha_{KL}$ so that rolls are stable for small ω. The results for $\phi = \phi_{max}$ give the threshold corresponding to Eq. (13), which is maximized over all orientations of perturbing rolls, while those for $\phi = -\theta$ give the theoretical threshold taking into account only those modes that can be accommodated in the computational box.

Rolls	r	α_2	Condition for stability		
			Numerics	Theory ($\phi = \phi_{max}$)	Theory ($\phi = -\theta$)
(3,4)	0.2	1.0	$\omega < 0.415 \pm 0.005$	$\omega < 0.406$	$\omega < 0.415$
(3,−4)	0.2	1.0	$\omega < 0.255 \pm 0.005$	$\omega < 0.255$	$\omega < 0.255$
(4,3)	0.3	0.5	$\omega < 0.655 \pm 0.005$	$\omega < 0.659$	$\omega < 0.660$
(4,−3)	0.3	0.5	$\omega < 0.555 \pm 0.005$	$\omega < 0.554$	$\omega < 0.564$

VI. NUMERICAL SIMULATIONS

In this section we present numerical simulations of the model (5), for infinite Prandtl number, and Eqs. (1) and (2), for finite Prandtl number. These simulations allow comparison with the analytical results presented above for various instabilities of the roll pattern, and also investigation into the nonlinear development of these instabilities, which is not otherwise amenable to the analysis. Our code is pseudospectral, and periodic boundary conditions are applied in both horizontal directions. In each simulation the computational box is square, with sides of length $L = 10\pi$. This size of box allows five pairs of rolls with critical wave numbers parallel to either side of the box. Adequate numerical resolution is obtained using 64×64 Fourier modes. Time stepping is achieved through the so-called exponential time differencing method [20].

We name rolls according to their orientation as follows: rolls with wave vector (k_1, k_2) are called $(k_1, k_2)L/2\pi$ rolls. For example, rolls with critical wave numbers and axes parallel to the y axis are (5,0) rolls, or, equivalently, (−5,0) rolls. Since (i,j) rolls are equivalent to $(-i,-j)$ rolls, we may specify that $i \geqslant 0$. This periodic computational box thus allows the following six critical rolls: (5,0), $(4,\pm 3)$, $(3,\pm 4)$, and (0,5) rolls, corresponding to $\theta = 0°$, $\theta \approx \pm 37°$, $\theta \approx \pm 53°$, and $\theta = 90°$, respectively.

The initial condition for each of our simulations takes the form of a roll pattern in one of these orientations added to a small random perturbation.

A. Infinite Prandtl number

First we simulate the infinite-Prandtl number model (5) for various values of r, ω, and α_2, fixing $\epsilon^2 = 0.2$, $\tau = 1$, and $\alpha_1 = -0.4$, and compare our results with those of Sec. III. We carry out two sets of simulations, distinguished by the stability of rolls when $\omega = 0$. In the first set, $\alpha_2 < \alpha_{KL} \approx 1.55$, and all rolls are stable to the Küppers-Lortz instability when $\omega = 0$; in the second set $\alpha_2 > \alpha_{KL}$, and all rolls are unstable when $\omega = 0$ (i.e., the stability curves have the topologies of Figs. 2(a) and 2(b), although the parameter values are different there from those appropriate here). For each initial orientation of the pattern, we carry out a series of simulations for different values of ω, noting where the stability of the roll pattern changes. Tables I and II summarize the results obtained from the various simulations. Note that the finite size of the computational box has the consequence that the theoretical stability boundary is shifted slightly, since perturbation rolls with $\phi = \phi_{max}$ are not generally permitted in the box, and it is more appropriate to compute the stability boundary using instead $\phi = -\theta$ (Table I) or the value $\phi = \phi_n$ corresponding to the most unstable mode found in our numerical simulations (Table II).

Consider first the simulations for $\alpha_2 < \alpha_{KL}$, corresponding to the parameter values in Table I. When $\omega = 0$, all rolls are stable, regardless of their orientation. The (5,0) rolls remain stable as ω is increased, but, as ω exceeds various threshold values, the $(3,\pm 4)$ and $(4,\pm 3)$ rolls are destabilized in turn. In our simulations, the nonlinear development of the instability reveals that they are eventually replaced by

TABLE II. Comparison between numerical and theoretical stability thresholds for rolls in various alignments, with $\alpha_2 > \alpha_{KL}$. As in Table I, the numerical stability thresholds are determined to within ± 0.005. The results for $\phi = \phi_{max}$ give the threshold corresponding to Eq. (13), which is maximized over all orientations of perturbing rolls, while those for $\phi = \phi_n$ give the theoretical threshold taking into account only the most unstable mode found in our numerical simulations, compatible with the finite computational box.

Rolls	r	α_2	Condition for stability		
			Numerics	Theory ($\phi = \phi_{max}$)	Theory ($\phi = \phi_n$)
(5,0)	0.2	2.0	$0.255 \leqslant \omega$	$0.283 \leqslant \omega$	$0.259 \leqslant \omega$
(3,4)	0.2	2.0	$0.265 \leqslant \omega \leqslant 0.425$	$0.327 \leqslant \omega \leqslant 0.425$	$0.307 \leqslant \omega \leqslant 0.425$
(5,0)	0.2	3.0	$0.515 \leqslant \omega$	$0.574 \leqslant \omega$	$0.570 \leqslant \omega$
(4,3)	0.2	3.0	$0.385 \leqslant \omega \leqslant 0.624$	$0.401 \leqslant \omega \leqslant 0.622$	$0.395 \leqslant \omega \leqslant 0.622$

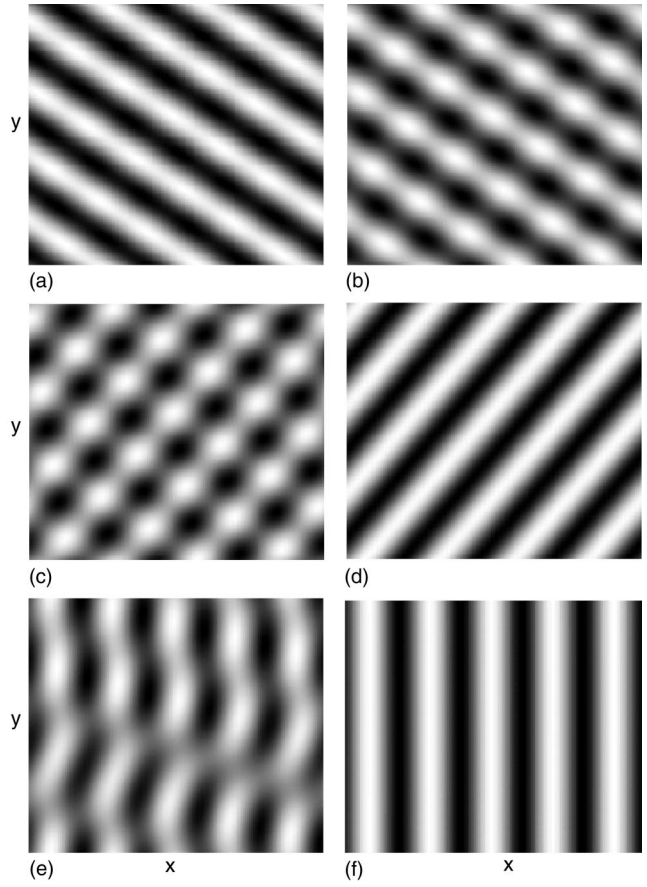

FIG. 6. Evolution of w in Eq. (5), with $\omega=0.425$ and $\alpha_2=2$. (a) (3,4) rolls at $t=0$. (b) Significant perturbation in the form of (4, -3) rolls at $t=11\,100$. (c) Rectangle pattern at $t=11\,450$. (d) (4, -3) rolls at $t=13\,900$. (e) Distorted rolls at $t=14\,250$. (f) (5,0) rolls at $t=16\,000$. In this case the final state of (5,0) rolls is stable.

a stable pattern of (5,0) rolls. Thus when ω is sufficiently large, rolls are forced to align with $\mathbf{\Omega}_h$, as one might expect.

By contrast, when $\alpha_2>\alpha_{\mathrm{KL}}$, all rolls are unstable to the Küppers-Lortz instability when $\omega=0$. Figure 5 shows the evolution of mode amplitudes over one cycle of the Küppers-Lortz instability for $\omega=0$ and $\alpha_2=2$ (cf. Ref. [13]). The initial state consists of (3,4) rolls; these are unstable to (1, -5) rolls, which themselves are unstable to (4,-3) rolls. In turn the (4,-3) rolls are replaced by (5,1) and then (3,4) rolls, thereby completing the cycle, which then repeats indefinitely, with a noise-dependent time scale determined by numerical precision. Note that the (1,-5) and (5,1) rolls do not have a critical wave number. Figure 6 shows the evolution of the pattern at $\omega=0.425$ from an initial state of (3,4) rolls. Here, these rolls are predicted to be unstable to perturbing rolls with $-96.7°\leqslant\phi\leqslant-73.8°$, and indeed we find in our simulations that the (3,4) rolls are eventually replaced by (4,-3)-rolls (which have $\phi=90°$). However, these rolls are themselves unstable (regardless of the value of ω when $\alpha_2=2$), and are eventually replaced by (5,0) rolls, which are stable. Figure 7 shows the corresponding evolution of the mode amplitudes.

For $\alpha_2>\alpha_{\mathrm{KL}}$, the stability boundary for rolls has a minimum at some $\theta>0$, and for sufficiently large values of α_2

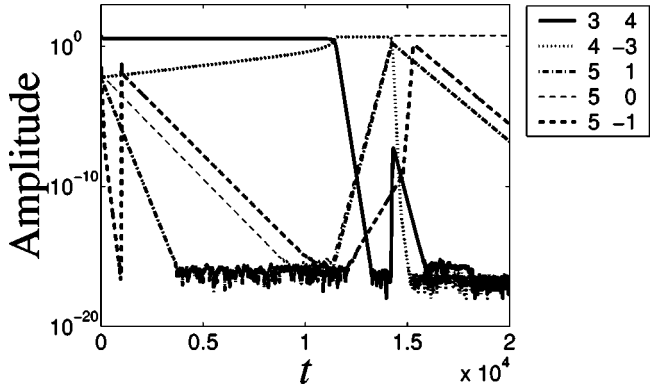

FIG. 7. Nonlinear evolution of mode amplitudes in Eq. (5), corresponding to Fig. 6. Instability of the initial (3,4) roll pattern to (4,-3) rolls manifests itself at $t\approx11\,400$. These rolls are ultimately replaced by stable (5,0) rolls.

this has the consequence that of the rolls permitted in our computational box, the first to become stabilized as ω is increased are not aligned with Ω_h. In order to confirm this prediction, we choose $\alpha_2=3$ and perform a set of simulations with an initial pattern of (5,0) rolls (i.e., rolls aligned with $\mathbf{\Omega}_h$). For small values of ω, we observe the Küppers-

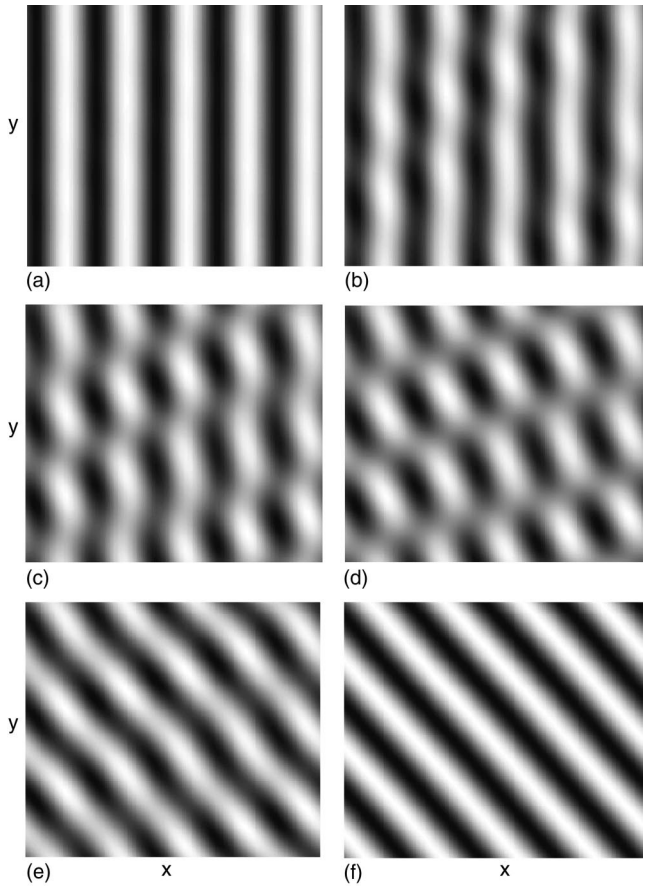

FIG. 8. Evolution of w in Eq. (5) for $\omega=0.4$ and $\alpha_2=3$. (a) (5,0) rolls at $t=0$. (b) Perturbed (5,0) rolls at $t=550$. (c) Wavy rolls at $t=700$. (d) Rectangular pattern at $t=750$. (e) Wavy (4,3) rolls at $t=800$. (f) Stable (4,3) rolls at $t=1000$.

Lortz instability, leading to an ever-repeating cycle similar to that illustrated in Fig. 5. However, when ω is sufficiently large, the result is qualitatively different, since some rolls become stable—the first rolls to be stabilized turn out to be the (4,3) rolls. In Fig. 8 we show the pattern evolution when $\omega=0.4$, during which the (5,0) rolls are ultimately replaced by stable (4,3) rolls, and there is no Küppers-Lortz cycle. As ω is increased further (i.e., above ≈ 0.515), the (5,0) rolls themselves become stable. These results are summarized in Table II, which shows the values of ω for which the (5,0) and (4,3) rolls are stable according to our analytical and numerical results: as ω is increased from zero, (5,0)-rolls are initially unstable, but become stable when ω exceeds some threshold. Rolls in any other orientation are initially unstable, then stabilize, then become unstable once more, and finally cease to exist as ω is increased [cf. Fig. 2(b)].

B. Finite Prandtl number

We now turn to finite-Prandtl-number simulations of Eqs. (1) and (2) to illustrate the influence of the small-angle and modulational instabilities on the convection pattern. Of course, these instabilities do not arise in isolation and in the process we also observe the more familiar skewed-varicose instability that is known to arise at finite Prandtl numbers [21,22]. Since many of our simulations produce qualitatively similar results, we illustrate them first with two sets of simulations, carried out for $\mathrm{Pr}=2$, and corresponding to a Taylor number of 1600. The parameter values are then: $\alpha_0=-0.398$, $\alpha_1=-0.3$, $\alpha_2=1.0$, $\alpha_3=8.273$, $\alpha_4=-3.670$, $\alpha_5=2.447$, $\alpha_6=-0.918$, and $\tau=1.034$. We also set $r=1$ and $\epsilon=0.3$. Each simulation has an initial state of (5,0) rolls with a small random perturbation.

When $\omega=0$, rolls are stable to the finite-angle form of the Küppers-Lortz instability, but unstable to the small-angle instability of Sec. IV A. Figure 9 shows the dominant mode amplitudes in this simulation, and Fig. 10 shows the corresponding evolution of the pattern. Initially the (5,1) and (5, -1) roll perturbations grow together, corresponding to the modes A_1 and A_2 in the theory of Sec. IV A, although neither has a critical wave number here. Eventually the (5,1) mode dominates and a pattern of (5,1) rolls ensues. This pattern is also unstable and is replaced in turn by (5,2) and then by (4,3) rolls. The (4,3) rolls are similarly unstable, this time to perturbations in the form of the (3,4) and (5,2) modes, This example can be related directly to the analysis of Sec. IV A, since both the initial rolls and one of the perturbing rolls have a critical wave number. Here, in the notation of that section, $k=\frac{4}{5}$ and $l=\frac{3}{5}$. The perturbation wave vectors differ from the wave vector of the initial rolls by $(m,n)=(-\frac{1}{5},\frac{1}{5})$. As in our infinite-Prandtl-number simulations at $\omega=0$, the orientation of the roll pattern continues to precess about the vertical, although the angle between successive rolls is much smaller here, leading to a generally wavier pattern, apparent in Fig. 10. Note that we are sufficiently far above onset that the participating rolls do not necessarily have critical wave numbers [e.g., the wave number of the (5,2) rolls is 1.077].

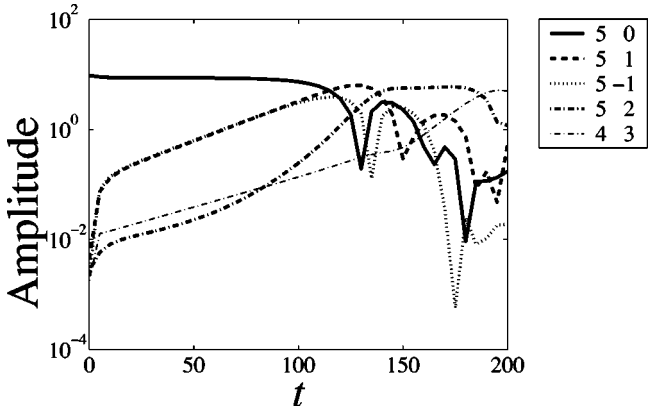

FIG. 9. Nonlinear evolution of the dominant mode amplitudes in Eqs. (1) and (2), when $\omega=0$. The initial (5,0) rolls are unstable to $(5,\pm 1)$ modes, which grow at almost identical rates, until eventually (at $t=125$), one perturbation wins, and a pattern of (5,1) rolls is obtained. These rolls are themselves unstable, and are replaced in turn by (5,2) rolls and (4,3) rolls.

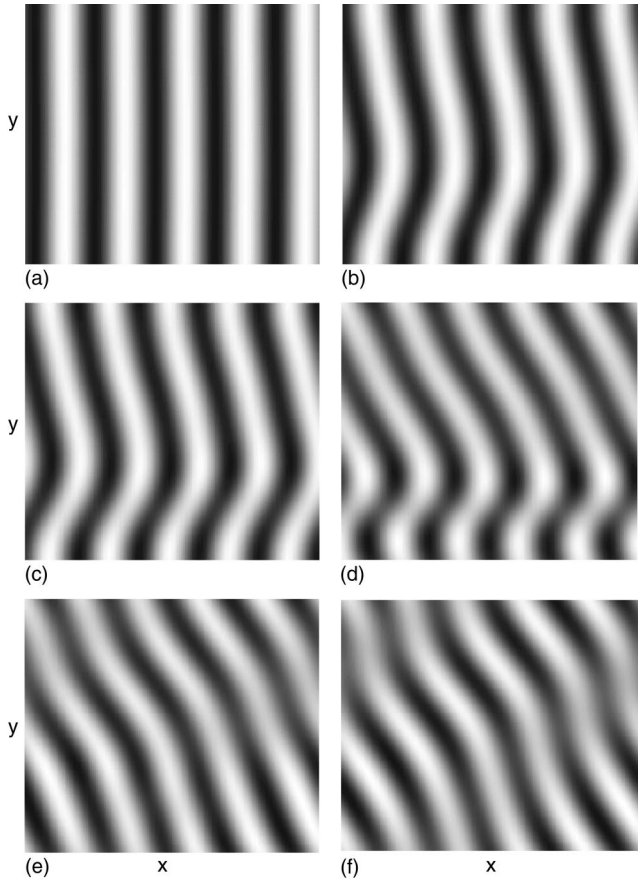

FIG. 10. Evolution of w in Eqs. (1) and (2) corresponding to Fig. 9. (a) (5,0) rolls at $t=0$. (b) Perturbed (5,0) rolls at $t=110$. (c) Wavy rolls at $t=120$. (d) Pattern at $t=150$. (e) Pattern at $t=170$. (f) Wavy (5,2) rolls at $t=180$.

For nonzero ω, some roll patterns become stabilized to these small-angle perturbations for sufficiently large ω, as they did in the infinite-Prandtl number case to the Küppers-Lortz instability, e.g., at $\omega=1.1$ the (4,3) rolls are stable. In a simulation from an initial state of (5,0) rolls, again at $\omega=1.1$ the pattern is initially replaced by (5,1) rolls; but these

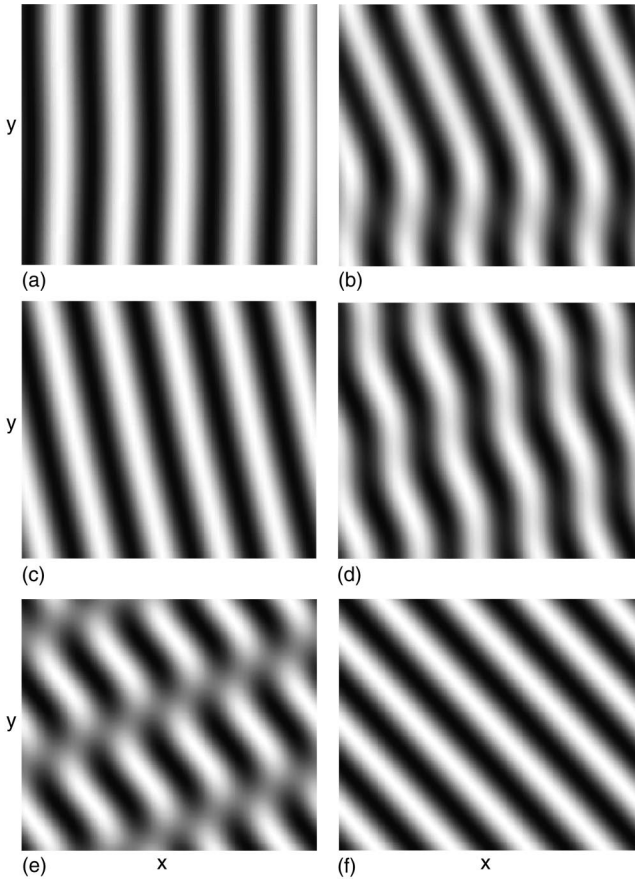

FIG. 11. Evolution of w in Eqs. (1) and (2) for $\omega=1.1$. (a) (5,0) rolls at $t=0$. (b) Wavy rolls at $t=30$. (c) (5,1) rolls at $t=50$. (d) Wavy (5,1) rolls at $t=90$. (e) Distorted rolls at $t=100$. (f) Stable (4,3) rolls at $t=110$.

rolls are unstable to small-angle perturbations, and eventually a stable (4,3) roll pattern is obtained. The evolution of this pattern is shown in Fig. 11. Note that the final steady pattern of rolls is not aligned with $\mathbf{\Omega}_h$. At even higher values of ω, the stable pattern is in closer alignment with $\mathbf{\Omega}_h$.

In our final set of simulations, we illustrate the effects of the modulational instability identified in Sec. V; to do so, we reduce Pr in order to satisfy Eq. (42). In all our simulations with $\omega=0$, we find that rolls become unstable to the small-angle instability before the predicted modulational instability can be observed (although we could clearly find this instability by restricting the perturbations to be parallel to the original rolls). The reason for this is the faster growth rate of the small-angle instability identified in Eq. (29). In order to eliminate the small-angle instability, the value of ω is increased; we find a value of $\omega=3$ to be sufficient. Results are shown for $\mathrm{Pr}=0.6$, $r=1$ and $\epsilon=0.5$ with an initial pattern consisting of (5,0)-rolls. For a Taylor number of 400 (so that $\alpha_0=-9\times10^{-3}$, $\alpha_1=-0.5$, $\alpha_2=1.0$, $\alpha_3=12.367$, $\alpha_4=-13.333$, $\alpha_5=8.889$, $\alpha_6=-0.999$, and $\tau=1.546$), we find that, while the (5,0) rolls are initially unstable to the skewed-varicose instability, this pattern itself becomes modulated in a manner analogous to that of the one-dimensional instability shown in Fig. 12(a). Eventually a one-dimensional, steady, modulated roll pattern, shown in Fig. 12(b), is obtained. At higher values of the vertical component of the rotation vector, a modulated skewed-varicose pattern [cf. Fig. 12(a)] is the final steady state of the system.

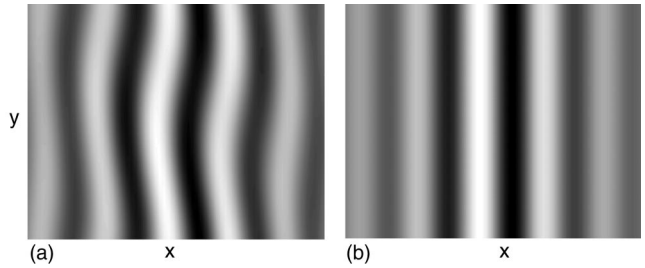

FIG. 12. Planforms of (a) a modulated skewed-varicose pattern and (b) a one-dimensionally modulated roll pattern. Parameter values are given in the text.

VII. CONCLUSIONS

In this paper we have studied the competing influences of the vertical and horizontal components of the rotation vector on the problem of pattern formation in thermal convection. Although this problem is of considerable geophysical relevance, it has received very little investigation in comparison with the case of a purely vertical rotation vector.

The horizontal component $\mathbf{\Omega}_h$ of the rotation vector breaks the orientational degeneracy of the problem, so that, in general, convection occurs in the form of rolls rather than more complicated patterns such as squares or hexagons. The rolls are subject to a competition between the Küppers-Lortz instability that leads to a continual precession of the roll axes, and the alignment instability that leads to a preference for rolls aligned with $\mathbf{\Omega}_h$. This competition can be analyzed within the framework of weakly nonlinear amplitude equations, provided that $|\mathbf{\Omega}_h|$ is small.

When the effects of the large-scale mean flow are negligible (e.g., in the limit of infinite Prandtl number), the problem can be studied with a single model equation (5). When the vertical rotation rate Ω_v is small, rolls are susceptible only to the alignment instability. A band of possible roll alignments exists, and within this band there is a smaller band of stable rolls. For larger Ω_v, the heteroclinic cycle associated with the Küppers-Lortz instability is broken, provided that $|\mathbf{\Omega}_h|$ is sufficiently large. There is then a band of stable rolls, but this band need not include rolls aligned with $\mathbf{\Omega}_h$; stable rolls can be aligned at an angle to $\mathbf{\Omega}_h$, so that the effects of the competing instabilities balance.

When the Prandtl number is finite, the problem is complicated by the presence of a neutral large-scale flow that greatly increases the range of potential instabilities of rolls. These large-scale instabilities include the small-angle form of the Küppers-Lortz instability [8,13], the skewed-varicose instability [19], and a one-dimensional amplitude-modulation instability [15,16]. The small-angle instability is not prevented by $\mathbf{\Omega}_h$, in the sense that almost all rolls within the band of existence remain unstable. Only a very narrow range of small-amplitude rolls near the edge of this band can be stable. We have not discussed in detail in this paper the

skewed-varicose instability, since its behavior is similar to the nonrotating case [18]. The one-dimensional instability is also unaffected by $\mathbf{\Omega}_h$.

We have conducted a sequence of numerical experiments to illustrate these various instabilities and to study their nonlinear development. The numerical results are consistent with the analytical predictions for the stability and instability of the rolls. In all cases, the instabilities evolve to a new state consisting of pure rolls of a different alignment or a heteroclinic cycle between roll states; there is no evidence of more complex steady-state patterns, such as wavy rolls. However, more complicated patterns are observed if the box size is increased, or if the simulations are carried out further from onset [8,12,18].

[1] G. Küppers and D. Lortz, J. Fluid Mech. **35**, 609 (1969).
[2] T. Clune and E. Knobloch, Phys. Rev. E **47**, 2536 (1993).
[3] M. Auer, F.H. Busse, and R.M. Clever, J. Fluid Mech. **301**, 371 (1995).
[4] F.H. Busse and M. Kropp, ZAMP **43**, 28 (1992).
[5] S. Chandrasekhar, *Hydrodynamic and Hydromagnetic Stability* (Oxford University Press, Oxford, 1961).
[6] F.H. Busse, Z. Naturforsch. A **37a**, 752 (1982).
[7] M. Kropp and F.H. Busse, Geophys. Astrophys. Fluid Dyn. **61**, 127 (1991).
[8] Y. Ponty, T. Passot, and P.L. Sulem, Phys. Rev. E **56**, 4162 (1997).
[9] P. Manneville, J. Phys. **44**, 759 (1983).
[10] M. Neufeld, R. Friedrich, and H. Haken, Z. Phys. B: Condens. Matter **92**, 243 (1993).
[11] S.M. Cox, SIAM (Soc. Ind. Appl. Math.) J. Appl. Math. **58**, 1338 (1998).
[12] A. Roxin and H. Riecke, Phys. Rev. E **65**, 046219 (2002).
[13] S.M. Cox and P.C. Matthews, J. Fluid Mech. **403**, 153 (2000).
[14] W. Eckhaus, *Studies in Non-Linear Stability Theory* (Springer, New York, 1965).
[15] P.C. Matthews and S.M. Cox, Nonlinearity **13**, 1293 (2000).
[16] S.M. Cox and P.C. Matthews, Physica D **149**, 210 (2001).
[17] M.R.E. Proctor, Phys. Lett. A **292**, 181 (2001).
[18] S.L. Pollicott, Ph.D. thesis, University of Nottingham, 2002 (unpublished).
[19] A. Zippelius and E.D. Siggia, Phys. Fluids **26**, 2905 (1983).
[20] S.M. Cox and P.C. Matthews, J. Comput. Phys. **176**, 430 (2002).
[21] F.H. Busse and R.M. Clever, J. Fluid Mech. **91**, 319 (1979).
[22] F.H. Busse and E.W. Bolton, J. Fluid Mech. **146**, 115 (1984).